INVESTIGATING THE ATOMIC INTERACTIONS OF FLEXIBLE ORGANIC SOLAR CELLS

Author: Jennifer Mejia Old Dominion University- Department of Chemistry

Abstract

Space applications of solar cells were initially implemented in the launch of NASA's Vanguard 1 in 1958. Since that time, solar technology has been integrated into the electrical power systems on the majority of spacecraft produced by NASA. Presently, top performing solar panels have reached record high efficiencies of 40% but require intricate and expensive manufacturing. The technology used to advance these systems also adds undesirable weight and restricts the diversity of their applications because of their rigidity. These limitations make promising alternatives, like organic solar cells (OSCs), viable options to investigate. While OSCs have great tunability, are lightweight, and currently optimized for 18% power conversions, efficiency is greatly limited by our ability to control their morphology. Specifically, our understanding of these materials on the atomic scale, relevant information for successful charge transport across the system, is limited by the technology available to characterize them. Here, we show how solid-state nuclear magnetic resonance (ssNMR) can be used to investigate important intermolecular interactions within OSC materials. The data obtained here, confirmed by X-ray diffraction (XRD), provide valuable insight into the competitive role that intermolecular interactions play in the packing patterns, a powerful performance indicator, observed in these systems.

1. Introduction

Solar panels are an integral power source for NASA spacecraft.[1] While current photovoltaic devices are the primary power sources used to complete missions, their heavier weights limit the amount of productive cargo, like fuel and instrumentation, that can be housed by these spacecrafts. Despite a variety of solar cell options, organic type solar cell (OSC) materials are merging to the forefront of viable alternatives because of their lighter weights and high specific power ratings.[2] Even with lower power conversion efficiencies compared to current systems, interest in this growing field has expanded in the last 20 years.[3]

Although variables like assembly technique and heat contribute to OSC performance, the "active layer" is arguably the largest area of opportunity for improvement.[4] This region in the solar cell, where light absorption and electron transport occurs, is typically comprised of mixtures of small organic molecules and conductive polymers.[5] Successful light absorption and charge transport are a product of the various atomic interactions between these mixtures.[6] As a result, molecules used in these cells are chosen because of their structural features, like π-π stacking, and potential charge carrying capacity.[7,8]

Unfortunately, the most common analytical methods for characterizing the active layer lack the spatial resolution required to deeply investigate the relationship between structure and function.[9] The complexity of these samples makes using more powerful techniques like x-ray diffraction (XRD) or solution nuclear magnetic resonance (NMR) extremely difficult.[10] Specifically, amorphous samples may not have the required long-range order for XRD and dissolving samples for solution NMR causes a total loss of structural features in cast cells. Consequently, developing new methodology to explore the unique structural features and potentially control the nanostructural morphology of the active layer is critical for improving their efficiencies.[11,12]

High resolution solid-state NMR (ssNMR) has been used for decades to characterize complex materials.[13–15] In solution NMR,

dissolved samples result in a single isotropic chemical shift caused by molecular tumblings in the solvent.[16] However, in ssNMR, no solvents are used, and samples are packed as-is into rotors for observation. Samples acquired in this manner have anisotropic interactions that are not averaged out like in solution NMR.[17] This is reflected in the broad lines of ssNMR spectra, where all possible orientations of molecules with respect to the external magnetic field are seen. Fortunately, with the use of advanced 2-D ssNMR techniques and spectral editing, these line broadening interactions provide useful information about the structure and dynamics of complex materials.[16]

Here, ssNMR was used to investigate the intermolecular interactions of various linear dialkyl N,N'-napthalene diimide (NDI) molecules. Since these compounds have excellent chemical, thermal, and optical abilities, they are an excellent prototype system for examination.[5,18] To perform the analysis, a series of NDIs were synthesized[19–21].

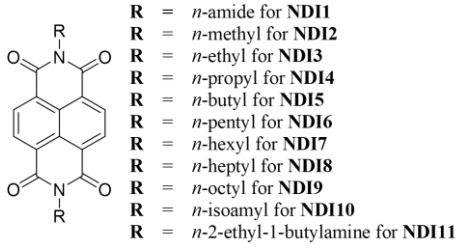

Figure 1. Chemical structure of NDIx molecules.

2. Experimental

2.1 Synthesis of the NDI compounds

All reagents used were commercially available and purchased through Sigma Aldrich. They were used as supplied without further purification.

N,N'-Diamide 1,4,5,8 naphthalenetetracarboxylic (NDI1) 1,4,5,8-Naphthalenetetracarboxylic dianhydride (0.51 g, 1.86 mmol) was dissolved in a stirred concentrated ammonium hydroxide (50 mL, 28 %, w/w) aqueous solution. Then, the mixture was stirred for 6 h at room temperature and a pale-yellow product diimide precipitate was obtained after vacuum filtration. The product was insoluble deuterated solvents and was characterized with solid-state NMR. ^{13}C NMR (100 MHz): δ 168.3, 164.61, 135.56, 127.33.

Synthesis of other N,N'-dialkyl-naphthalene diimide compounds were prepared according to modified literature procedures:[20]

A slurry of naphthalenetetracarboxylic dianhydride (0.5 g, 1.86 mmol) in 25 mL of N,N-dimethylformamide was treated with 2 equivalents of each primary amine. The homogenous mixture was sealed in a pressure vessel and heated at 80 °C for 1 hour and then cooled. The resulting slurry was diluted with several volumes of methanol and filtered. The solid was washed with methanol and air dried. All NDIs displayed spectral characteristics consistent with their assigned structures.

N,N'-Dimethyl-1,4,5,8-naphthalenetetracarboxylic diimide (NDI2) ^{1}H NMR (400 MHz, $CDCl_3$): δ 8.81 (s, 4H), 3.63 (s, 6H).

N,N'-Diethyl-1,4,5,8-naphthalenetetracarboxylic diimide (NDI3) ^{1}H NMR (400 MHz, $CDCl_3$): δ 8.79 (s, 4H), 4.31 (q, 4H), 1.39 (t, 6H).

N,N'-Dipropyl-1,4,5,8-naphthalenetetracarboxylic 1,8:4,5-diimide (NDI4) ^{1}H NMR (400 MHz, $CDCl_3$): δ 8.78 (s, 4H), 4.22 (m, 4H), 1.82 (m, 4H), 1.06 (t, 6H).

N,N'-Dibutyl-1,4,5,8-naphthalenetetracarboxylic diimide (NDI5) ^{1}H NMR (400 MHz, $CDCl_3$): δ 8.78 (s, 4H), 4.25 (m, 4H), 1.76 (m, 4H), 1.49 (m, 4H), 1.02 (t, 6H).

N,N'-Dipentyl-1,4,5,8-naphthalenetetracarboxylic diimide (NDI6) ^{1}H NMR (400 MHz, $CDCl_3$): δ 8.78 (s, 4H), 4.22 (m, 4H), 1.78 (m, 4H), 1.44 (m, 8H), 0.95 (t, 6H).

N,N'-Dihexyl-1,4,5,8-naphthalenetetracarboxylic diimide (NDI7) ^{1}H NMR (400 MHz, $CDCl_3$): δ 8.78 (s, 4H), 4.22 (m, 4H), 1.77 (m, 4H), 1.46 (m, 4H), 1.37 (m, 8H), 0.92 (t, 6H).

N,N'-Diheptyl-1,4,5,8-naphthalenetetracarboxylic diimide (NDI8) ^{1}H NMR (400 MHz, $CDCl_3$): δ 8.77 (s, 4H), 4.23 (m, 4H), 1.76 (m, 4H), 1.42 (m, 8H), 1.32 (m, 8H), 0.90 (t, 6H).

N,N'-Dioctyl-1,4,5,8-naphthalenetetracarboxylic diimide (NDI9) ^{1}H NMR (400 MHz, $CDCl_3$): δ 8.78 (s, 4H), 4.24 (m, 4H), 1.77 (m, 4H), 1.30 (m, 20H), 0.90 (t, 6H).

N,N'-Diisopentylamine-1,4,5,8-naphthalenetetracarboxylic diimide (NDI10) ^{1}H NMR (400 MHz, $CDCl_3$): δ 8.78 (s, 4H), 4.24 (m, 4H), 1.776 (m, 2H), 1.6 (m, 4H), 1.06 (d, 12H).

N,N'-Di2-ethyl-1butylamine-1,4,5,8-naphthalenetetracarboxylic diimide (NDI10) ^{1}H NMR (400 MHz, $CDCl_3$): δ 8.78 (s, 4H), 4.17 (m, 4H), 1.97 (m, 2H), 1.41 (m, 6H), 1.41 (m, 6H), 0.96 (m, 12H).

2.2 Instrumentation

Solution-state NMR

Solution-state NMR analyses were performed using a Bruker Avance III 400 spectrometer at 400 MHz for ^{1}H. The NDI samples were dissolved in deuterated chloroform, and then transferred into a 5-mm NMR tube. A 1D proton spectrum was acquired with 64 scans and 1s delay.

Solid-state NMR spectroscopy

All ^{13}C NMR analyses were performed on a Bruker Avance II 400 spectrometer at 100 MHz for ^{13}C. Samples were packed in 4-mm-diameter zirconia rotors with Kel-F caps, and experiments were run in a double-resonance probe head and the rotor was spun at the magic angle of 54.7° to the direction of the magnetic field. The ^{13}C chemical shifts were referenced to tetramethylsilane (TMS), with ^{13}COO-labeled glycine at 176.49 ppm as a secondary reference.

X-ray Crystallography

Crystals of **NDI2** and **NDI10** suitable for X-ray analyses were grown by solvent diffusion from chloroform solution. All measurements were made by Robert D. Pike of William and Mary University in Williamsburg, VA using microfocus Cu Kα radiation on a Bruker-AXS three-circle Apex DUO diffractometer, equipped with a SMART Apex II CCD detector. The full dataset was collected at 100 K or 296 K.

Crystal structures of **NDI1**, **NDI3**, **NDI5**, **NDI7**, and **NDI9** were found in the CSD database[22–30]

3. Results and Discussion

3.1 Crystal Structures

NDIs were categorized using 1D ssNMR and their corresponding crystal structures. Correlation was determined using: (1) symmetry, (2) bulk packing, and (3) intermolecular forces. All NDIs had either

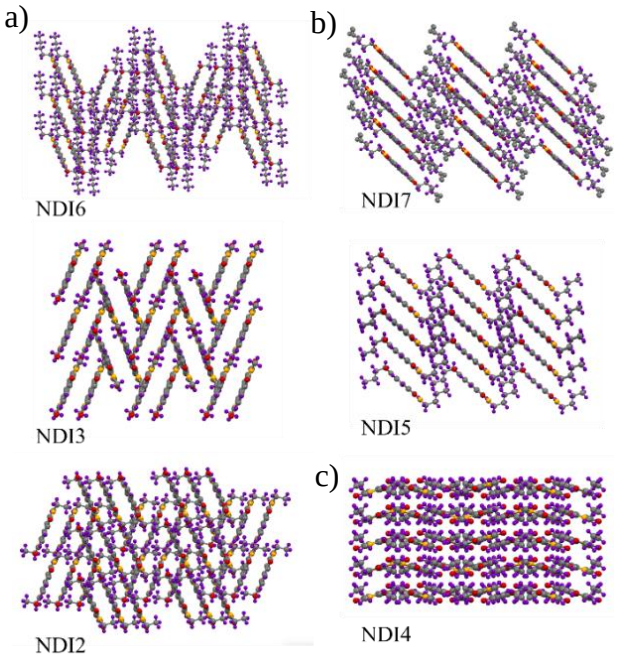

Figure 2. a) bidirectional planar packing b) monodirectional planar packing, c) zigzag packing

monoclinic or triclinic crystal systems, except for **NDI4** that was orthorhombic. Crystal structures show that the bulk packing of these NDIs had a similar relationship, with all straight, alkane derivatized systems falling into three categories. First, NDIs with monoclinic symmetry had bidirectional planar packing. Furthermore, NDIs with triclinic or orthorhombic symmetry had monodirectional planar and zigzag packing, respectively (Figure 2).

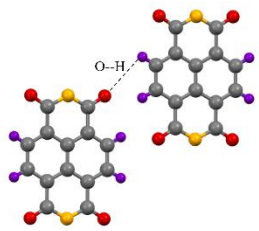

Figure 3. Intermolecular hydrogen bonding between columnar stacks of NDIs

Regardless of packing types, all NDIs formed columns, or chains via π-π and intermolecular forces. Specifically, crystal structure data provided insight regarding intermolecular hydrogen bonding between aromatic hydrogen and carbonyl oxygen atoms of adjacent stacks NDIs, whether monoclinic or triclinic of lower alkane chain lengths, had stronger intermolecular polar covalent O-H bonding between columns of in-plane adjacent molecules (Figure 3). The precursor material, 1,4,5,8-naphthalenetetracarboxylic dianhydride had the weakest hydrogen bonding with distances of 3.547 Å (Table 1). Whereas the first NDI of the series, **NDI1**, had higher bond strength with intermolecular O-H distances of 2.606 Å. It was observed that methyl additions resulted in progressively stronger attraction with **NDI7** having the greatest attraction with the shortest distance of 2.388 Å. After **NDI7** though, lengthening the alkane chain weakened this hydrogen bonding. This is reflected with an increased distance seen in **NDI9** and beyond.

3.2 ^{13}C multiple cross-polarization magic angle spinning (multiCP/MAS) NMR

The effect of these crystal structure packing patterns was observed with 1D ssNMR. For each of the NDIs, both saturated and electronegative groups presented as predicted and there were no notable patterns. However, aromatic regions of the 1D spectra did mirror the patterns observed in NDI crystal structures.

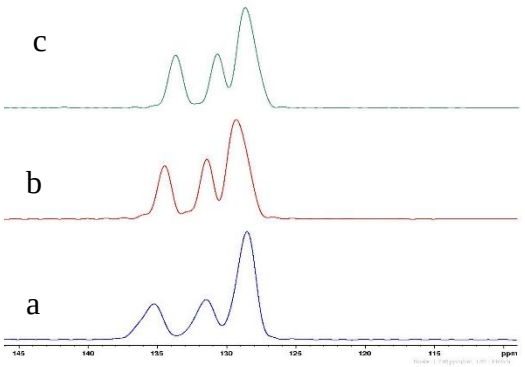

Figure 4. 1D ssNMR of (a) NDI2, (b) NDI3, and (c) NDI6

Similarities to the features governing packing were determined using peak shapes, resolution, and chemical shifts. Using these relationships, four NMR types of the straight chain NDIs was observed: (A) monoclinic, bidirectional planar packing with stronger O-H attraction (B) triclinic, monodirectional planar packing with stronger O-H attraction, (C) orthorhombic, zigzag packing with weaker O-H attraction, and (D) triclinic, monodirectional planar packing with weaker O-H attraction.

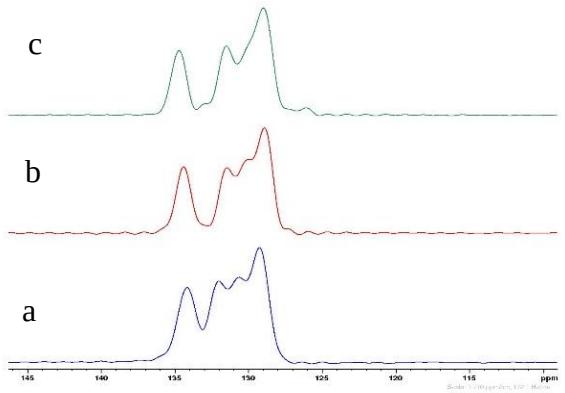

Figure 5. 1D ssNMR of (a) NDI5, (b) NDI7, and (c) NDI8

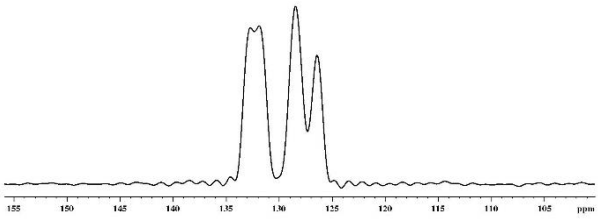

Figure 6. 1D ssNMR of NDI9

Table 1. Crystal structure, packing, intermolecular hydrogen bonding, and 1D NMR summary

Compound	Space group	Stacking	O-H (Å)	Bulk packing	1D NMR
NDI1	P-1	II	2.606	Monodirectional	F
NDI2	$P2_1/c$	III	2.416	Bidirectional	A
NDI3	$P2_1/c$	III	2.390	Bidirectional	A
NDI4	Pbca	IV	2.541	Zigzag	C
NDI5	P-1	III	2.452	Monodirectional	B
NDI10	P-1	III	2.367	Monodirectional	A
NDI6	$P2_1/n$	III	2.454	Bidirectional	A
NDI7	P-1	III	2.388	Monodirectional	B
NDI8	unknown	-	-	-	B
NDI9	P-1	III	2.464	Monodirectional	D
Other work	P-1	III	2.584	Monodirectional	-
Other work	P-1	III	3.035	Monodirectional	-
Other work	P-1	III	3.035	Monodirectional	-
NDI11	unknown	-	-	-	B

1D ssNMR spectra of **NDI10** and **NDI11** showed some deviation from the patterns observed with straight chain NDIs. **NDI10**, while, triclinic and monodirectional, had NMR patterns like the type A, bidirectional NDIs. Additionally, **NDI11**, showed similarities to type B NMR spectra. The crystal structure for **NDI11** is still unknown.

3.3 Two-dimensional ^{1}H-^{13}C heteronuclear correlation (2D HETCOR) NMR

Molecular interactions and further characterization of the NDI aromatic environments were probed using high resolution ssNMR. Correlation of ^{13}C chemical shifts with ^{1}H chemical shifts can reveal more structural information than 1D ^{13}C or ^{1}H spectra. Since ^{1}H-^{13}C dipolar couplings can provide correlation between internuclear distances of about 6 Å, 2D HETCOR NMR is able to reveal proximities of different functional groups.

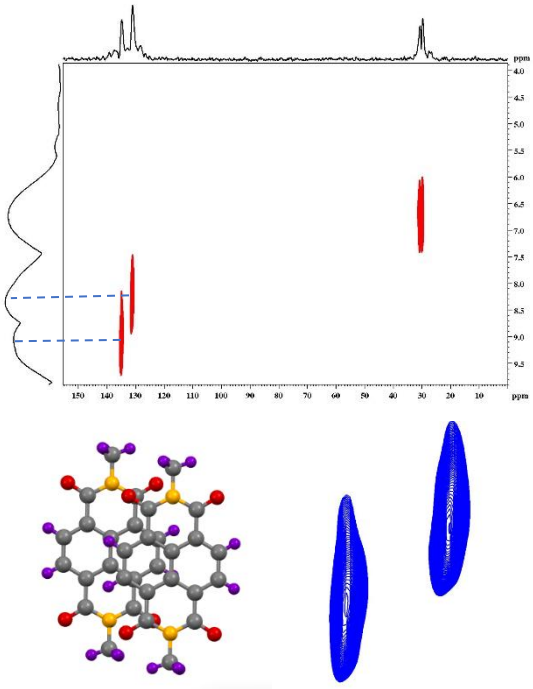

Figure 7. HETCOR and stacking of NDI2 with two aromatic proton peaks

Here, HETCOR spectra provided insight into the effects of columnar stacking on the NDIs. For many of the HETCOR spectra, each NDI had through space correlation to two,

not one aromatic protons. This diverges from the information obtained using solution NMR where all NDIs had equivalent aromatic environments in ^{1}H spectra. For some NDIs, only one aromatic proton was observed. These experimental anomalies were explained using crystal structure data, Each NDI, **NDI2**, **NDI3**, **NDI5**, **NDI6**, **NDI7**, **NDI9**, **NDI10**, and **NDI11** had similar displaced columnar stacking. **NDI1** and **NDI4** did not stack like the others and had different HETCOR spectra. The effects that chain length and intermolecular forces impose has impacts on the chemical environments that each of the aromatic protons are exposed to.

For those molecules with two aromatic peaks, crystal structure data show that the offset packing creates two different environments, explaining the two peaks in each of the HETCOR spectra.

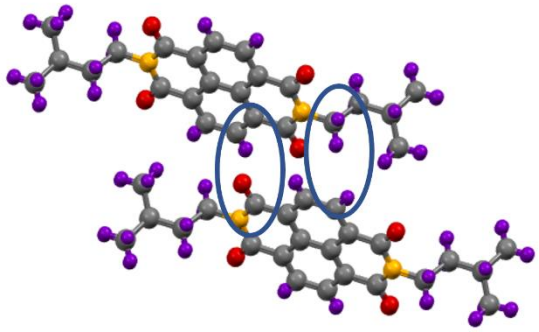

Figure 8. Top-down column packing of NDI11. Circles indicate different environments. One proton is closest to the alkyl chain and the other is surrounded by carbonyls.

This packing breaks the symmetry of the chemical environment and results in two different magnetic fields within the aromatic system versus what originally was thought to be one.

4. Conclusions

Since molecules observed using ssNMR lack position averaging from tumbling in solvents like solution NMR, the spectra reflect the local packing and chemical environment via through space couplings. It was found that

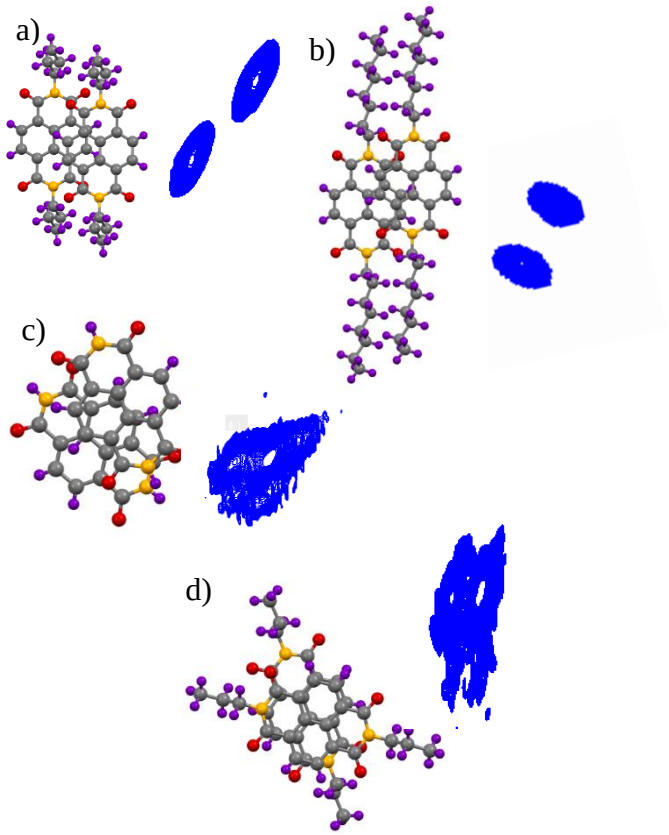

Figure 9. HETCOR aromatic peaks and stacking of (a) NDI5, (b) NDI9, (c) NDI1, and (d) NDI4.

both 1D ssNMR and 2D HETCOR provided information on how structural features may impact the packing and resulting potential performance of a molecule in an OSC.

References:

(1) Green, C. M.; Lomask, M. *Project Vanguard: The NASA History*, Dover ed.; Dover Publications: Mineola, N.Y, 2009.

(2) Reb, L. K.; Böhmer, M.; Predeschly, B.; Grott, S.; Dreißigacker, C.; Drescher, J.; Meyer, A.; Müller-Buschbaum, P. An Experiment for Novel Material Thin-Film Solar Cell Characterization on Sounding Rocket Flights. *Review of Scientific Instruments* **2021**, *92* (7), 074501. https://doi.org/10.1063/5.0047346.

(3) Chen, L. X. Organic Solar Cells: Recent Progress and Challenges. *ACS Energy Lett.* **2019**, *4* (10), 2537–2539. https://doi.org/10.1021/acsenergylett.9b02071.

(4) 25th Anniversary Article: Bulk Heterojunction Solar Cells: Understanding the Mechanism of Operation - Heeger - 2014 - Advanced Materials - Wiley Online Library https://onlinelibrary.wiley.com/doi/abs/10.1002/adma.201304373 (accessed 2022 -04 -09).

(5) Nowak-Król, A.; Shoyama, K.; Stolte, M.; Würthner, F. Naphthalene and Perylene Diimides – Better Alternatives to Fullerenes for Organic Electronics? *Chem. Commun.* **2018**, *54* (98), 13763–13772. https://doi.org/10.1039/C8CC07640E.

(6) Benanti, T. L.; Venkataraman, D. Organic Solar Cells: An Overview Focusing on Active Layer Morphology. *Photosynth Res* **2006**, *87* (1), 73–81. https://doi.org/10.1007/s11120-005-6397-9.

(7) Li, H.; Sini, G.; Sit, J.; Moulé, A. J.; Bredas, J.-L. Understanding Charge Transport in Donor/Acceptor Blends from Large-Scale Device Simulations Based on Experimental Film Morphologies. *Energy Environ. Sci.* **2020**, *13* (2), 601–615. https://doi.org/10.1039/C9EE03791H.

(8) Menke, S. M.; Ran, N. A.; Bazan, G. C.; Friend, R. H. Understanding Energy Loss in Organic Solar Cells: Toward a New Efficiency Regime. *Joule* **2018**, *2* (1), 25–35. https://doi.org/10.1016/j.joule.2017.09.020.

(9) Bryce, D. L. NMR Crystallography: Structure and Properties of Materials from Solid-State Nuclear Magnetic Resonance Observables. *IUCrJ* **2017**, *4* (4), 350–359. https://doi.org/10.1107/S2052252517006042.

(10) Vanlaeke, P.; Swinnen, A.; Haeldermans, I.; Vanhoyland, G.; Aernouts, T.; Cheyns, D.; Deibel, C.; D'Haen, J.; Heremans, P.; Poortmans, J.; Manca, J. V. P3HT/PCBM Bulk Heterojunction Solar Cells: Relation between Morphology and Electro-Optical Characteristics. *Solar Energy Materials and Solar Cells* **2006**, *90* (14), 2150–2158. https://doi.org/10.1016/j.solmat.2006.02.010.

(11) Nieuwendaal, R. C.; Snyder, C. R.; DeLongchamp, D. M. Measuring Order in Regioregular Poly(3-Hexylthiophene) with Solid-State 13C CPMAS NMR. *ACS Macro Lett.* **2014**, *3* (2), 130–135. https://doi.org/10.1021/mz4005343.

(12) Measuring the Degree of Crystallinity in Semicrystalline Regioregular Poly(3-hexylthiophene) | Macromolecules https://pubs.acs.org/doi/10.1021/acs.macromol.6b00799 (accessed 2022 -04 -09).

(13) Mao, J.; Cao, X.; Olk, D. C.; Chu, W.; Schmidt-Rohr, K. Advanced Solid-State NMR Spectroscopy of Natural Organic Matter. *Progress in Nuclear Magnetic Resonance Spectroscopy* **2017**, *100*, 17–51. https://doi.org/10.1016/j.pnmrs.2016.11.003.

(14) Mao, J.; Kong, X.; Schmidt-Rohr, K.; Pignatello, J. J.; Perdue, E. M. Advanced Solid-State NMR Characterization of Marine Dissolved Organic Matter Isolated Using the

Coupled Reverse Osmosis/Electrodialysis Method. *Environ. Sci. Technol.* **2012**, *46* (11), 5806–5814. https://doi.org/10.1021/es300521e.

(15) R. Luginbuhl, B.; Raval, P.; Pawlak, T.; Du, Z.; Wang, T.; Kupgan, G.; Schopp, N.; Chae, S.; Yoon, S.; Yi, A.; Jung Kim, H.; Coropceanu, V.; Brédas, J.; Nguyen, T.; Reddy, G. N. M. Resolving Atomic-Scale Interactions in Nonfullerene Acceptor Organic Solar Cells with Solid-State NMR Spectroscopy, Crystallographic Modelling, and Molecular Dynamics Simulations. *Advanced Materials* **2022**, *34* (6), 2105943. https://doi.org/10.1002/adma.202105943.

(16) Duer, M. J. *Introduction to Solid-State NMR Spectroscopy*; Blackwell: Oxford, UK ; Malden, MA, 2004.

(17) Levitt, M. H. *Spin Dynamics: Basics of Nuclear Magnetic Resonance*, 2nd ed.; John Wiley & Sons: Chichester, England ; Hoboken, NJ, 2008.

(18) Ye, L.; Zhao, W.; Li, S.; Mukherjee, S.; Carpenter, J. H.; Awartani, O.; Jiao, X.; Hou, J.; Ade, H. High-Efficiency Nonfullerene Organic Solar Cells: Critical Factors That Affect Complex Multi-Length Scale Morphology and Device Performance. *Adv. Energy Mater.* **2017**, *7* (7), 1602000. https://doi.org/10.1002/aenm.201602000.

(19) Ofir, Y.; Zelichenok, A.; Yitzchaik, S. 1,4;5,8-Naphthalene-Tetracarboxylic Diimide Derivatives as Model Compounds for Molecular Layer Epitaxy. *J. Mater. Chem.* **2006**, *16* (22), 2142–2149. https://doi.org/10.1039/B601258B.

(20) Shukla, D.; Welter, T. R. N-Type Semiconductor Materials in Thin Film Transistors. WO2009126203A1, October 15, 2009.

(21) Iscrulescu, L.; Sebe, I.; Atanasoaie, D.; Tantaveanu, E.; Mîndruta, C. New Xanthene Structures. *Revista de Chimie* **2008**, *59* (5), 578–0.

(22) Meillaud, F.; Shah, A.; Droz, C.; Vallat-Sauvain, E.; Miazza, C. Efficiency Limits for Single-Junction and Tandem Solar Cells. *Solar Energy Materials and Solar Cells* **2006**, *90* (18), 2952–2959. https://doi.org/10.1016/j.solmat.2006.06.002.

(23) Pandeeswar, M.; Khare, H.; Ramakumar, S.; Govindaraju, T. Biomimetic Molecular Organization of Naphthalene Diimide in the Solid State: Tunable (Chiro-) Optical, Viscoelastic and Nanoscale Properties. *RSC Adv.* **2014**, *4* (39), 20154–20163. https://doi.org/10.1039/C3RA47257D.

(24) Krishna, G. R.; Devarapalli, R.; Lal, G.; Reddy, C. M. CCDC 1029340: Experimental Crystal Structure Determination, 2016. https://doi.org/10.5517/CCDC.CSD.CC13K3J9.

(25) Alvey, P. M.; Reczek, J. J.; Lynch, V.; Iverson, B. L. A Systematic Study of Thermochromic Aromatic Donor−Acceptor Materials. *J. Org. Chem.* **2010**, *75* (22), 7682–7690. https://doi.org/10.1021/jo101498b.

(26) Andric, G.; Boas, J. F.; Bond, A. M.; Fallon, G. D.; Ghiggino, K. P.; Hogan, C. F.; Hutchison, J. A.; Lee, M. A.-P.; Langford, S. J.; Pilbrow, J. R.; Troup, G. J.; Woodward, C. P. CCDC 238148: Experimental Crystal Structure Determination, 2005. https://doi.org/10.5517/CC7ZT66.

(27) Shukla, D.; Nelson, S. F.; Freeman, D. C.; Rajeswaran, M.; Ahearn, W. G.; Meyer, D. M.; Carey, J. T. Thin-Film Morphology Control in Naphthalene-Diimide-Based Semiconductors: High Mobility n-Type Semiconductor for Organic Thin-Film

Transistors. *Chem. Mater.* **2008**, *20* (24), 7486–7491. https://doi.org/10.1021/cm802071w.

(28) Milita, S.; Liscio, F.; Cowen, L.; Cavallini, M.; Drain, B. A.; Degousée, T.; Luong, S.; Fenwick, O.; Guagliardi, A.; Schroeder, B. C.; Masciocchi, N. Polymorphism in *N* , *N* ′-Dialkyl-Naphthalene Diimides. *J. Mater. Chem. C* **2020**, *8* (9), 3097–3112. https://doi.org/10.1039/C9TC06967D.

(29) Alvey, P. M.; Reczek, J. J.; Lynch, V.; Iverson, B. L. CCDC 819750: Experimental Crystal Structure Determination, 2011. https://doi.org/10.5517/CCWJ0KY.

(30) Lynch, D. E.; Hamilton, D. G. CCDC 230429: Experimental Crystal Structure Determination, 2004. https://doi.org/10.5517/CC7QS6X.